

Evaluation of solar irradiance at the surface—inferences from in situ and satellite observations and a mesoscale model

Thara Prabha · Gerrit Hoogenboom

Received: 1 March 2009 / Accepted: 1 July 2010 / Published online: 27 August 2010
© Springer-Verlag 2010

Abstract Accurate information about the solar irradiance at the soil surface is essential for many agricultural, hydrological and environmental models that take into account the surface energy balance. The main goal of present study was to evaluate the solar irradiance predictions from the Advanced Research Weather Research and Forecasting (ARW) model for both clear sky and cloudy conditions. An extended observational dataset from the Georgia Automated Environmental Monitoring Network (AEMN) provided hourly solar irradiance at the surface and other collocated surface level measurements. The radiation bias (determined from the difference between the ARW predictions and AEMN observations) showed a linear relationship with the cloud optical depth and the cirrus cloud amount from the moderate resolution imaging spectroradiometer (MODIS). For cloud-free days, the ARW model had a positive radiation bias that exceeded 120 W m^{-2} over coastal and urban areas of Georgia. The model radiation and air temperature bias increased with increasing aerosol optical depth derived from the MODIS observations during the cloud-free days, attributed to fire events that lasted intermittently throughout the study period. The model biases of temperature,

mixing ratio, wind speed, and soil moisture were linearly dependent on the radiation bias.

1 Introduction

Solar irradiance data (incoming solar flux at the surface) is an integral component of meteorology, air quality assessments, ecophysiological, hydrological, and biophysical models, and solar power generation (Brutsaert 1982; Iqbal 1983). Solar radiation measurements are often sparse at many locations (Thornton and Running 1999) and models are either physically based on well established radiative transfer equations or on empirical methods. Empirical methods are based on latitude, altitude, solar elevation angle, amount of precipitable water, atmospheric turbidity, surface albedo (LeBaron and Dirmhirn 1983; Soler 1990), which is typically adopted in various applications. The amount of solar radiation at the surface is closely dependent on the presence of clouds and representation of clouds in the radiation models cause most uncertainties. Empirical methods for estimating solar radiation do not account for the effect of imminent large-scale weather systems or the influence from meso-locale scale weather circulations due to land surface discontinuities or uneven terrain, which can also cause cloudiness and rain.

The convective precipitation events common in Georgia and other southeastern states during the spring and summer months are often local, intense, and with short duration, compared to a frontal system that has wide spread cloudiness and rain. This scenario introduces a high spatial and temporal variability in the cloud amount and in the radiation received at the surface. High-resolution meso- and local scale numerical models, such as the advanced weather research and forecasting (ARW) model (<http://www.wrf-model.org>), account for the physics and dynamics of the

T. Prabha · G. Hoogenboom
Department of Biological and Agricultural Engineering,
The University of Georgia,
Griffin, GA 30223-1797, USA

T. Prabha (✉)
Indian Institute of Tropical Meteorology (IITM),
Dr. Homi Bhabha road, Pashan,
Pune-8, India
e-mail: thara@tropmet.res.in

Present Address:
G. Hoogenboom
AgWeatherNet,
Washington State University,
Prosser, WA 99350-8694, USA

atmosphere, radiative divergence and cloud processes and surface atmosphere interactions (Skamarock et al. 2005). High-resolution predictions from meso-local scale models is invaluable in providing advisories and assessments, as location-specific information can be made available from the model in advance. Although the use of high-resolution weather predictions in agriculture has added advantage due to the spatial and temporal information, there is imminent need for the evaluation of the high-resolution predictions. Model evaluation studies often include surface sensible parameters such as temperature, wind speed and relative humidity (Betts et al. 1997; Beljaars et al. 1996; Chen et al. 2007; Ek et al. 2003; Cheng and Steenburgh 2005). However, evaluation of radiation fluxes is rare due to the scarcity of observations over several spatially distinct point observations. It should be emphasized that collocated datasets of radiation and temperature from mesonet networks or from the National Weather Service can be used effectively to find the underlying causes for model failures.

Radiative forcing under clear sky conditions are also influenced by the amount of water vapor and aerosol (Trishchenko and Li 1998). The accuracy of the high-resolution models in predicting the surface layer weather heavily depends on the accuracy of the surface energy balance and thereby on the solar irradiance. Zamora et al. (2003) showed that incoming solar irradiance errors can impact the performance of the numerical model MM5. They discussed the impact of radiative transfer parameterization errors and their effects on mesoscale weather predictions. Dudhia (1989) found that incorrect representation of aerosol scattering and absorption, and ozone absorption in the model can lead to positive errors of approximately 100 W m^{-2} in the instantaneous total solar irradiance at the surface. Guichard et al. (2003) evaluated the MM5 shortwave radiation from a 10-km nested domain against the Atmospheric Radiation Measurement Program dataset over the southern Great Plains for a period of 70 days. The lack of representation of aerosol radiative effects attributed to biomass burning (Peppler et al. 2000) and an underestimation of cirrus and low cloud amount were responsible for the overestimation of solar irradiance at the surface by the model. Zamora et al. (2003) showed that the clear sky solar irradiance errors can have a significant impact on numerical model performance. The ARW model is the next generation model that is ‘the first fully compressible conservative form nonhydrostatic atmospheric model designed for both research and operational NWP applications’ (Skamarock et al. 2005). So far, no radiation evaluation studies using the WRF-ARW model have been reported in the literature. The relationship between the temperature or mixing ratio errors and the radiation biases especially needs to be addressed.

The Georgia Automated Environmental Monitoring Network (AEMN; www.georgiaweather.net) provides concurrent spatial and temporal information on the shortwave radiative

flux, soil conditions, and surface sensible weather parameters such as temperature, mixing ratio, wind speed, etc. The main goal of current study was to evaluate the downward/solar irradiance at the surface predicted by the ARW model against several observations over Georgia recorded by the AEMN. The main objective of the study was to determine the role of radiation errors in contributing to errors in the near surface temperature, water vapor mixing ratio, wind, soil temperature predictions during both cloudy and cloud-free conditions.

2 Materials and methods

2.1 WRF model configuration

The Advanced Research WRF model (ARW V2.2, Skamarock et al. 2005) was used in this study. There are two different physical parameterization options for shortwave radiation in the ARW V2.2 model used in this study (more options for radiation parameterizations are available in the newer releases of ARW). The first one is the MM5 scheme (Dudhia 1989) that incorporates the effects of clear air scattering, water vapor absorption, and cloud albedo and absorption, however, no aerosol effects are included in this version. The second one is the Goddard scheme with 11 spectral bands that incorporates the effects of cloud, carbon dioxide, and ozone absorption. Both are one-dimensional schemes in which model equations are solved for each column separately. Community Atmosphere Model radiation scheme (which allows inclusion of aerosol and trace gas effects) was also later implemented and was not available during this study. The MM5 shortwave parameterizations based on Dudhia (1989) is used in the present study; it calculates the downward shortwave flux as,

$$S_d(z) \cong \mu S_0 - \int_z^{\text{top}} (dS_{cs} + dS_{ca} + dS_s + dS_a) \quad (1)$$

Where, z is height above the surface, μ is cosine of the solar zenith angle, S_0 is the solar constant, dS_{cs} , dS_{ca} , dS_s , and dS_a are cloud scattering/reflection, cloud absorption, clear air scattering, and water vapor absorption, respectively. It is to be noted that aerosol effects are not considered.

All model runs in the present study were configured to have the same parameterization options. A description of the ARW model and physics parameterizations is available at http://www.mmm.ucar.edu/wrf/users/docs/arw_v2.pdf. The Yonsei University Planetary Boundary Layer scheme coupled with the Monin Obukhov similarity for the surface layer and Noah land surface scheme (Chen and Dudhia 2001a, b) were used. Also, the WRF Single Moment 3-class (WSM3) microphysics, Kain Fritsch cumulus param-

eterization, Rapid Radiative Transfer Model longwave parameterization were used. Details of these physics options in ARW are described in the technical manual (see http://www.mmm.ucar.edu/wrf/users/docs/arw_v2.pdf for more details). The model runs were conducted with two, two-way interactive nested grids at 9 km, and 3 km resolutions. Forty vertical pressure levels were considered with finer resolution close to the surface, which accommodated approximately 15 vertical levels in the boundary layer. The outer domain incorporated Georgia and parts of all neighboring states, while the inner 3 km domain mainly covered the state of Georgia. All model runs were initialized with the North American Regional Reanalysis (NARR) data (Mesinger et al. 2006), which were available at a 32-km spatial resolution. The boundary of the outer domain was updated with NARR data every 3 h. The sea surface temperature was also updated accordingly at the same interval. However no reinitializations were done.

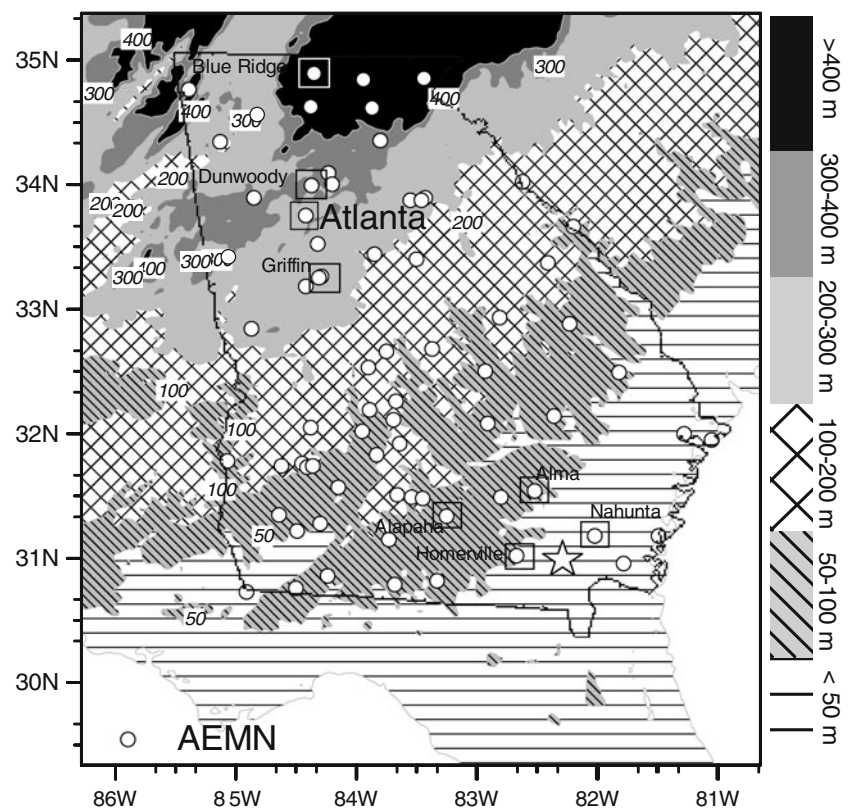
2.2 Data and methods

The year 2007 was one of the worst drought years in Georgia and was characterized by a significant reduction in precipitation. Two separate ARW model runs were conducted; the first one used the ARW version 2.2 for the run for April, May, and June 2007, while the second run was conducted with ARW version 2.2.1 for the month of July,

2007. The study period was influenced by a forest fire in the southeastern Georgia and northern Florida. However, most of the impact from the fire occurred during the month of May. The month of July was dominated with more cloudy conditions and less influence from the fire. To investigate the role of cloudiness, data from July without the influence of forest fires were considered.

The Georgia AEMN (Fig. 1) encompasses over 75 stations across the state of Georgia (Hoogenboom 2005) over a widely varying terrain with contrasting surface elevation, landuse and soil characteristics. Routine measurements of surface wind, air temperature, relative humidity, surface pressure, solar radiation, net radiation (at selected stations), rainfall, volumetric soil moisture content, and soil temperatures at depths of 5, 10, and 20 cm are available at 15-min intervals (Hoogenboom 2005). The LI200X pyranometer (Campbell Scientific, Inc., Logan, Utah, USA) calibrated for the 400–1,100 nm spectrum is used in the AEMN network. Calibrations of the LI200X pyranometer were conducted against four LICOR transfer standard pyranometers under Metal Halide lamps. The transfer standards were calibrated to the Kipp and Zonen CM21. These calibrations are carried out regularly for all sites and periodic checks are carried out daily using surrounding weather stations. LI200X's are mounted at a height of 3.2 m facing upper hemisphere and are not obscured. Suspected sites contaminated by shadow

Fig. 1 Topography of domain 2 and the AEMN surface meteorological stations. The location of the fire is indicated with a *star*



effects of overgrown trees were removed from the analysis. Maintenance of each weather station and its sensors is performed every 6 to 8 weeks and the quality of the data are checked daily. Hourly data derived from this network were used for comparison studies with model data archived at hourly intervals. The AEMN data provided an independent evaluation for model results since the AEMN are not associated with the reanalysis data used for model initialization.

The ARW setup in the present study involved two domains, one nested inside the large domain. The topography of the region in domain 2 is presented in Fig. 1. To determine the role of topography, observational data were grouped into six classes based on station elevation as >400 m, 300–400 m, 200–300 m, 100–200 m, 50–100 m and <50 m classes. Mean bias (difference between the ARW model grid point value and observations) for each hourly period was found for each terrain. Data from 68 stations were considered for this study, with 5, 3, 13, 16, 23, and 8 stations in classes 1 to 6, respectively. The cloudy and clear days were analyzed separately in detail.

2.2.1 Analysis for the cloudy days

Measurements of solar irradiance at the surface were available at several AEMN stations. However, collocated cloudiness data were not available. So it was necessary to adopt methodologies to attain cloudiness information. Two different methods were used to account for the impact of clouds on radiation bias. In the first approach, cloud optical thickness and cirrus reflectance data from Moderate Resolution Imaging Spectroradiometer (MODIS) Level II cloud data at 5 km resolution were used. The MODIS cloud data were extracted for all AEMN locations. The scan time of the satellite was approximately 1000 LST. The model biases for radiation and temperature for all AEMN locations and at 1000 LST were obtained and aggregated into bins of cloud optical thickness and cirrus reflectance. It should be noted that only data from July were considered for this analysis to isolate the influence on the radiation biases from clouds. Also, this method only deals with 1000 LST biases. 33.5% of the cloud optical depth data from MODIS were missing during this period for the locations that were evaluated.

MODIS data were only available once daily. To estimate the cloudiness for the other times during the day, we used a second approach. In this approach, clear sky estimates of solar incoming flux were estimated using the first term of Eq. 1, without accounting for atmospheric effects due to clouds, water vapor or clear air. The deviation from this clear sky flux and the solar irradiance at the surface observation was considered as a measure of cloudiness and other effects that lead to a reduction in the solar

irradiance at the surface. ‘Clear sky’ data selection was conducted by the aggregation of cases with minimum difference ($<10 \text{ W m}^{-2}$) between the clear sky estimate (R_c) and the AEMN observations (R_o). To study the effect of cloudiness on model performance, a fractional cloudiness (F_c) was defined as,

$$F_c = \frac{R_c - R_o}{\max(R_c - R_o)} \quad (2)$$

2.2.2 Analysis for cloud-free days

Cloud-free days data were analyzed separately to study the impact of other factors that might be responsible for the difference between the model and observations. MODIS Level II Aerosol Optical Depth (AOD) data at 10 km spatial resolution were used. Corrected AOD (Remer et al. 2005) data at AEMN locations during the forest fire were used with model radiation and 2 m temperature biases.

Concurrent measurements of temperature, wind speed, relative humidity, and surface pressure along with surface solar irradiance measurements at AEMN locations allowed us to investigate model surface temperature, humidity, wind, soil temperature prediction errors in association with radiation errors. Data during the period 900–1700 LST were considered. The radiation bias for every hour was determined from the difference between the ARW predictions and AEMN observations and was averaged in respective bins of hourly temperature bias (AEMN-ARW).

3 Results

An example for four different good, bad, and worst scenarios that are contributing to the discrepancy between the ARW model predictions and observations are presented in Fig. 2a–d using data for the weather station located in Alapaha (see Fig. 1). A clear day, e.g., June 11, presented in Fig. 2a showed the least model bias (model-AEMN $\approx 25 \text{ W m}^{-2}$). Figure 2b shows a comparison between model predictions and observations for a partly cloudy case, e.g., July 26. Although the model was able to predict the variation in radiation very accurately in response to cloudiness, biases were double compared to those found for the clear sky case (Fig. 2a) and this appears to be due to insufficient cloudiness in the model. Figure 2c shows a case for July 20 where the model predicted cloudiness was less than the observations for the morning hours and more than the observations for the afternoon hours. Positive bias in the morning hours indicates that there is more irradiance in the model and fewer clouds compared to observations. For a worst case scenario for the morning hours, such as the one

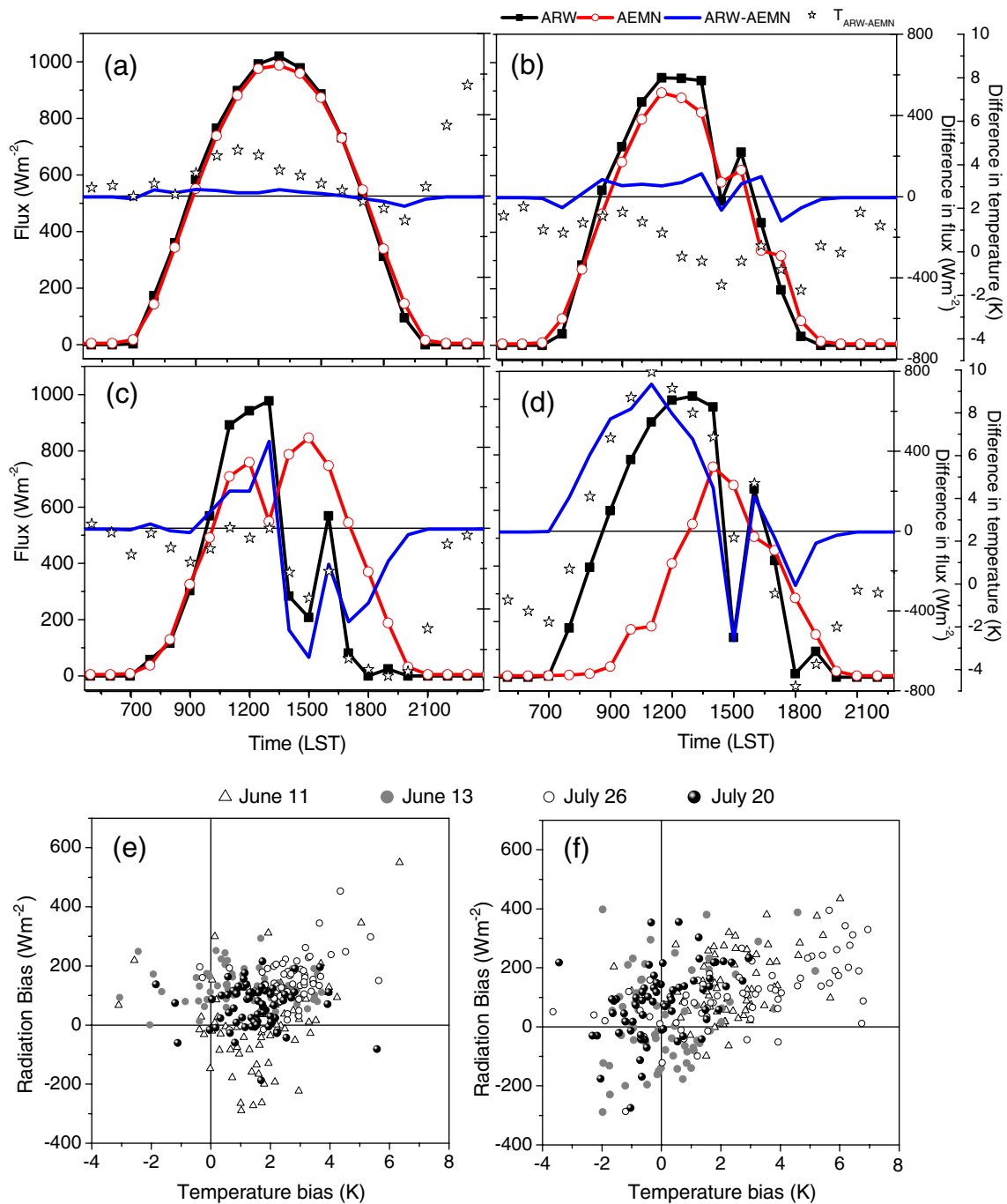


Fig. 2 Comparison between ARW predicted and AEMN observed incoming solar radiation for Alapaha for good to worst scenarios; a cloud-free day on June 11 (a), a partly cloudy day on July 26 (b) a model overcast day on July 20 (c) and an overcast day with rain on June 13 (d). The relationship between temperature bias and radiation

bias for the AEMN stations for the morning with correlation coefficient less than 0.3 (e) and afternoon (f) hours on 4 days (correlation coefficients 0.29, 0.33, 0.61, and 0.41, respectively, for 4 days considered)

for an overcast day, e.g., June 13, with a total of 101 mm accumulated rainfall during a 24-h period, the bias exceeded $\pm 700 W m^{-2}$ (Fig. 2d). The negative bias in the afternoon indicated less radiation in the model compared to observations which means that model predicted afternoon cloudiness was higher than the observed cloudiness.

The 2-m temperature bias showed a stronger correlation ($r \approx 0.3-0.6$) with the radiation bias in the afternoon hours and was stronger for the overcast days. The relationship between radiation and temperature biases during the morning (700–1200 LST) and afternoon (1300–1800 LST) were examined separately for the 4 days presented in Fig. 2e–f

for all AEMN stations. Each point in the Fig. 2e–f corresponds to average solar radiation bias for the individual AEMN stations for one of the 4 days considered in Fig. 2a–d. These results suggested that 2 m level temperature errors in the model were closely related to solar irradiance errors for most of the stations. The relationship between the errors for radiation and temperature were stronger for most stations during the afternoon hours, compared to the morning hours and for cloudy days.

3.1 Effect of terrain

To summarize the results from all stations, the individual station data were grouped into different terrain classes (Fig. 1) for the remainder of this study. A terrain class with elevation less than 50 m includes all coastal stations. A reduction ($40\text{--}80\text{ W m}^{-2}$) in the average solar radiation for the lowest elevation (terrain height less than 50 m) was found for the AEMN observations. The 300–400 m terrain classification, including the urban stations around Atlanta, also showed a similar reduction in the solar radiation compared to other terrain classes. However, the model

predictions did not show such a difference over the coastal areas and there was only a slight reduction in the radiation for the 300–400 m terrain class predicted by the model. It should be emphasized that aerosol effects were not included in the radiation model used here. The differences seen could be attributed to forest fire emissions in the low-lying region in south Georgia. The fire emissions caused episodic dimming effects at the surface, where irradiance at the surface was lesser than for a clear conditions and temperature had reduced (Prabha and Hoogenboom 2009). These aspects will be discussed in Section 3.3 on cloud-free cases.

The model bias for the four months April, May, June, and July 2007 against observations for the six terrain classes are presented in Fig. 3. During April, a maximum model bias (140 W m^{-2}) was found when the elevation was less than 50 m and greater than 300 m. The difference in bias among different locations increased with time and peaked at 1100 LST, which could possibly be attributed to various factors such as the development of clouds due to the initiation of convection, and the amount of water vapor and pollutants in the atmosphere. For the coastal stations, the development and progression of the sea breeze front

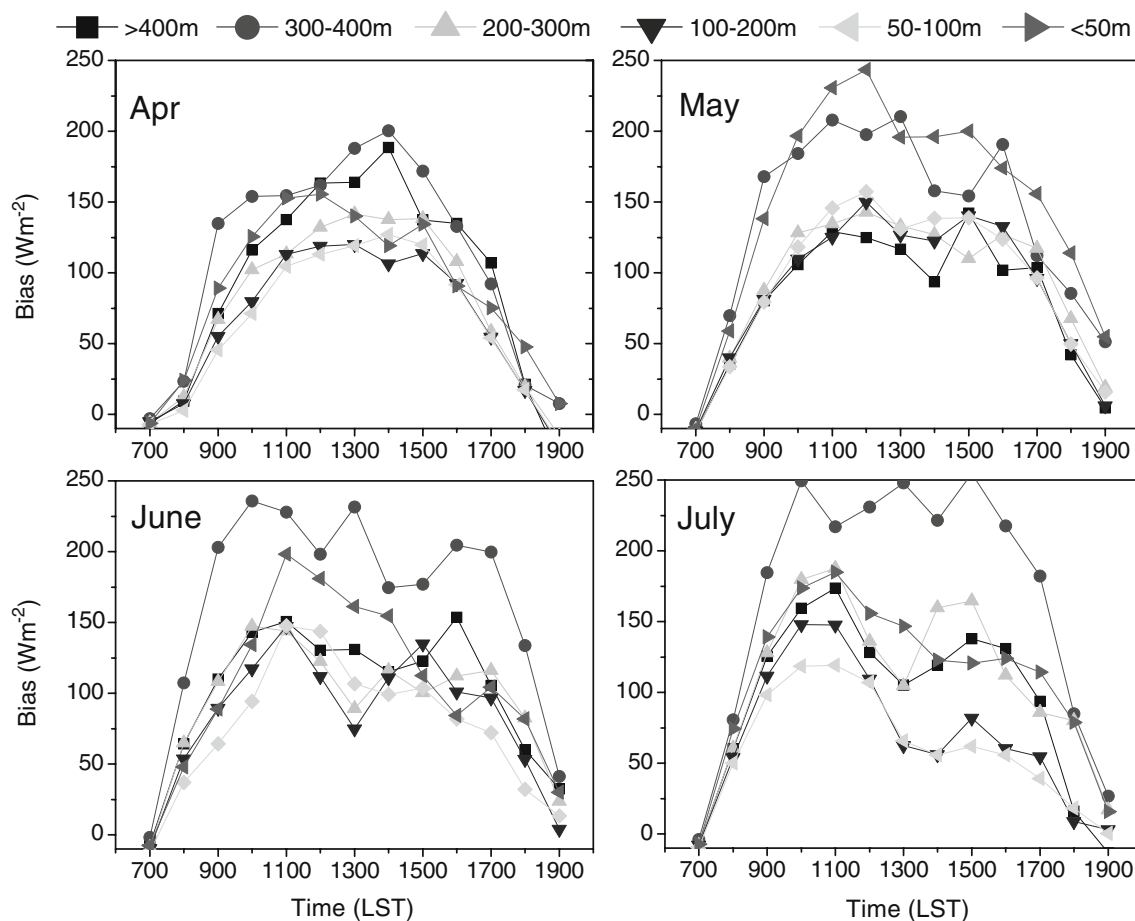


Fig. 3 Hourly bias in the solar radiation predictions of the ARW model when compared to the observations of the Georgia Automated Environmental Monitoring Network for six elevation classes, averaged by month

and associated convergence and cloud formation that followed was important. On several instances, the ARW model has reproduced convergence zones for areas further inland in south Georgia and for the coastal areas to the east. A reduction in radiation biases around the noon hours also indicated that clouds associated with the shallow convection were present in the model, associated with early convection than in the observations. However, there was a secondary peak for model bias at 1500 LST, as shallow clouds dissipated and that lead to less radiation. The stations in the low-lying areas with an elevation less than 50 m indicated a doubling of radiation bias during the month of May, which was attributed to other possible causative effects such as forest fires present at this location. It should be noted that there were no wild fires in south Georgia during the month of July. However, the month of May was significantly affected by wild fires. During July, the morning radiation bias was considerably higher, with a maximum of $\approx 120\text{--}180\text{ W m}^{-2}$ for all locations and with peaks of 240 W m^{-2} for urban area.

3.2 Effect of cloudiness

The hourly variation in the shortwave radiation depended strongly on the amount of cloudiness and the spatial variability was considerable (Fig. 2). Since hourly observations of cloudiness were not available at AEMN locations, MODIS cloud optical thickness (COT) during the month of July was used to evaluate the role of clouds. However, MODIS data are only available during the scan time of the satellite, which happens at 1000 LST. Nearly 33% of data were missing, which means that not all station data for all valid AEMN observations could be included in this analysis.

Integrated cloud water from the ARW simulations (not presented) increased with COT from MODIS, indicating that the model accounted for the observed variation in cloud water. Binned solar irradiance at the surface bias (ARW-AEMN) averaged for all stations and for the month of July is presented as a function of cloud optical thickness in Fig. 4a. There were positive and also occasional negative biases at individual stations; however a positive bias dominated for most stations. The positive radiation bias increased with the cloud optical thickness obtained from MODIS. Model bias varied from 70 to 200 W m^{-2} with increasing COT from 1 to 60 (Fig. 4a). These results also showed an increase in the 2 m temperature bias from 0.5 to 3 K with increasing COT from 1 to 60. The bin-averaged bias for the urban and coastal areas, i.e. second (300–400 m) and sixth (<50 m) elevation classes showed higher biases from $150\text{--}300\text{ W m}^{-2}$ in response to a dependence on the COT from 1 to 60 (Fig. 4a).

The low-level clouds might have caused most of the radiation bias. However, the availability of cirrus reflection from MODIS allowed us to check the performance of the

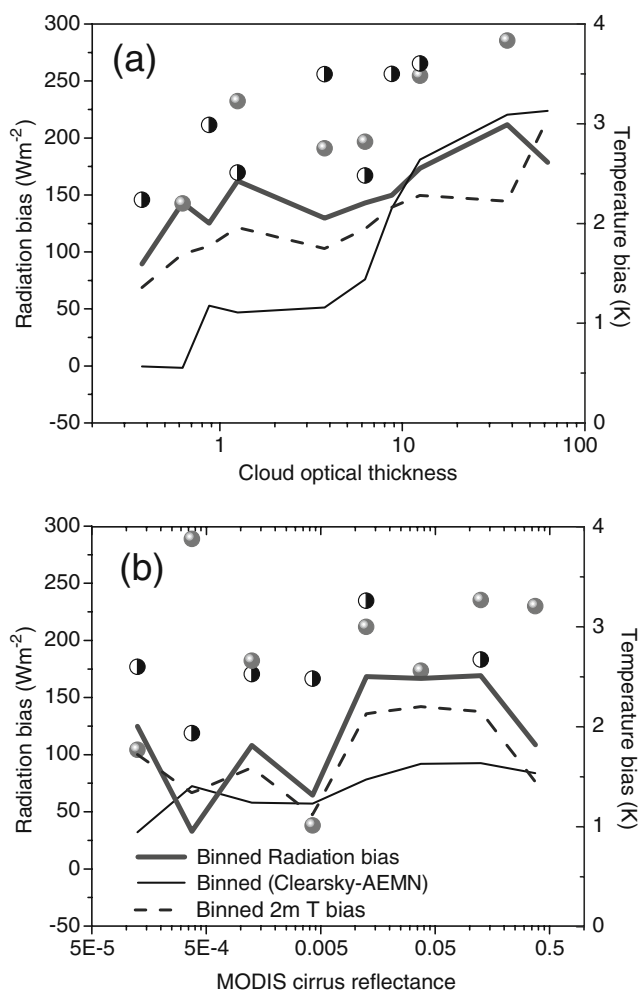


Fig. 4 Radiation bias as function of cloud optical thickness (a) and cirrus reflectance (b) from MODIS. Filled circles and half-filled circles indicate radiation biases corresponding to AEMN stations in the sixth (<50 m) and second (300–400 m) elevation classes, respectively

model under different cirrus reflectance conditions to look at the role of high clouds (Fig. 4b). The radiation bias (ARW-AEMN) averaged for all stations and for the month of July showed only a slight dependence on the cirrus reflectivity. Higher positive biases existed for low values of COT and cirrus reflectivity over the urban and coastal areas compared to other locations.

The COT obtained from MODIS was only available for the passing time of the satellite. Therefore, we adopted a second approach with a cloud fraction (F_c) to assess hourly cloudiness information based on AEMN solar irradiance at the surface measurements. This cloud fraction was based on the difference between the clear sky estimate and the observed solar irradiance at the surface ($R_c - R_o$). It is expected that ($R_c - R_o$) has a similar relationship with COT or cirrus reflectance as that of the radiation bias. ($R_c - R_o$) for 1000 LST was obtained for each station and grouped into

different MODIS COT and cirrus reflectance bins (Fig. 4a and b). The comparison of actual radiation bias and the ($R_c - R_o$) showed a good agreement for a high COT (>10), indicating that this measure of cloudiness is more representative when COT was high. In a strict sense, ($R_c - R_o$) will include the attenuation of solar irradiance at the surface due to clouds, water vapor or pollutants in the atmosphere, which may explain the disparity at low COTs.

($R_c - R_o$) showed a strong impact due to cloudiness at higher elevations and at locations with the lowest elevation that were close or in the coastal areas (Fig. 5a). Maximum cloudiness at locations in the 200–400 m elevation emphasized the importance of leeside cyclogenesis southeast of the Appalachian Mountains. It is also very likely attributed to the Sandhills circulation (Raman et al. 2005), which might play a significant role in the initiation of convection and formation of clouds in this region.

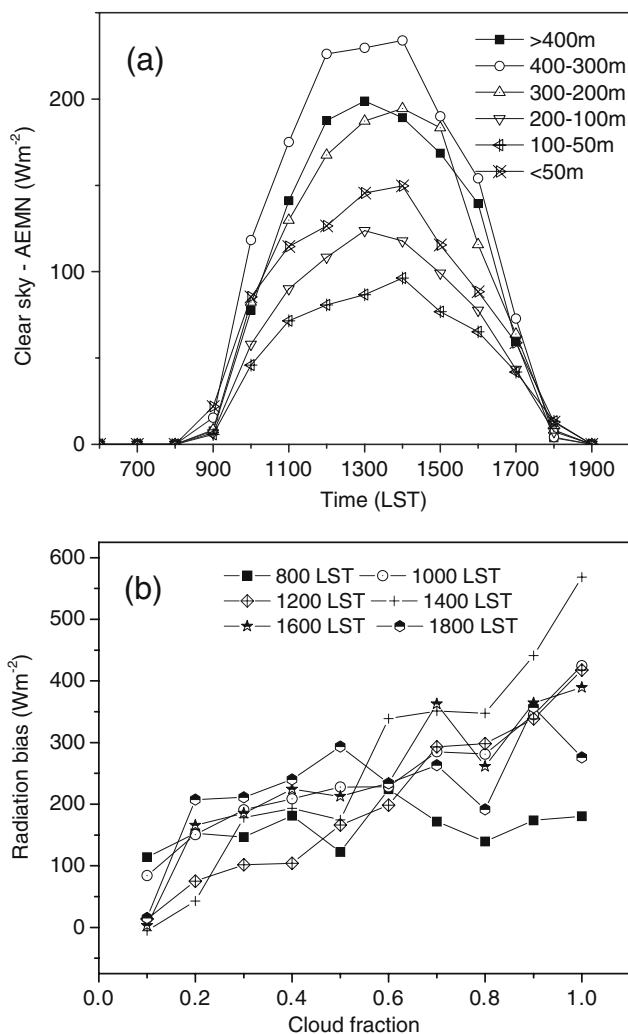


Fig. 5 Difference between the estimated clear sky downward radiation and the AEMN observation for different terrain elevation classes during the month of July 2007 (a) and dependence of solar radiation bias on cloud fraction for different times during the day (b)

Previously, episodic experiments have shown that the aerosol radiative forcing at the top of the atmosphere could not be discarded for cities like Atlanta (Carrico et al. 2003). This type of urban contribution due to aerosols and other pollutants, such as aerosols and ozone, might also have contributed to large values of ($R_c - R_o$) for the urban areas (300–400 m elevation class). Aerosols can attenuate the solar irradiance at the surface through scattering and absorption. Absorbing aerosols, especially carbonaceous ones can also affect cloud radiative properties and precipitation (Hansen et al. 1997; Rosenfeld and Lensky 1998; Kaufman et al. 2002; Ramanathan et al. 2001; Gustafson et al. 2006). There was only a minimum influence from the clouds in the locations with elevation 50–200 m with a mean difference in radiation fluxes that was less than 120 W m⁻². The increased values along coastal areas were a result of the meso-gamma scale circulations associated with the sea breeze convergence as a result of increased heating in July. An estimate of the cloud fraction derived from this analysis at different times of the day and associated radiation bias (Fig. 5b) for 800 LST and 1000 LST showed a minimum bias of 90–100 W m⁻² corresponding to zero fractional cloud cover. This suggests an inherent positive model bias during the morning hours. There was a linear relationship between the amount of cloudiness and model bias, with the highest bias for overcast cases. r^2 between the cloud fraction and radiation bias during 900–1700 LST was 0.98. The representation of boundary layer clouds in the parameterization scheme chosen is another issue that could be important here. The Kain Fritsch cumulus parameterization was used, which assumes that all clouds in the grid cell are of the same type.

Using the clear sky estimate as described earlier, the radiation bias for the cloudy and clear conditions during the month of May, i.e., heavily influenced by forest fires, and July, i.e., forest fires were absent, was examined. The highest elevation and lowest elevation areas showed a maximum bias during the clear cases (Fig. 6a–b). The clear conditions during May exhibited a maximum value between 1000 and 1500 LST, with 50–100 W m⁻² at locations with elevation 50–100 m and 125 W m⁻² at coastal areas. However, during July, a positive bias was noticed mainly for the morning hours and differences with observations either vanished or became negative during the afternoon hours. The radiation bias increased considerably during the cloudy cases of May and July (Fig. 6c–d), with a maximum value for May that exceeded 350 W m⁻². To address this issue, the cloud-free cases were studied separately.

3.3 Cloud-free cases

The relationship of radiation with terrain, cloudiness did not explain the discrepancies between the model predicted

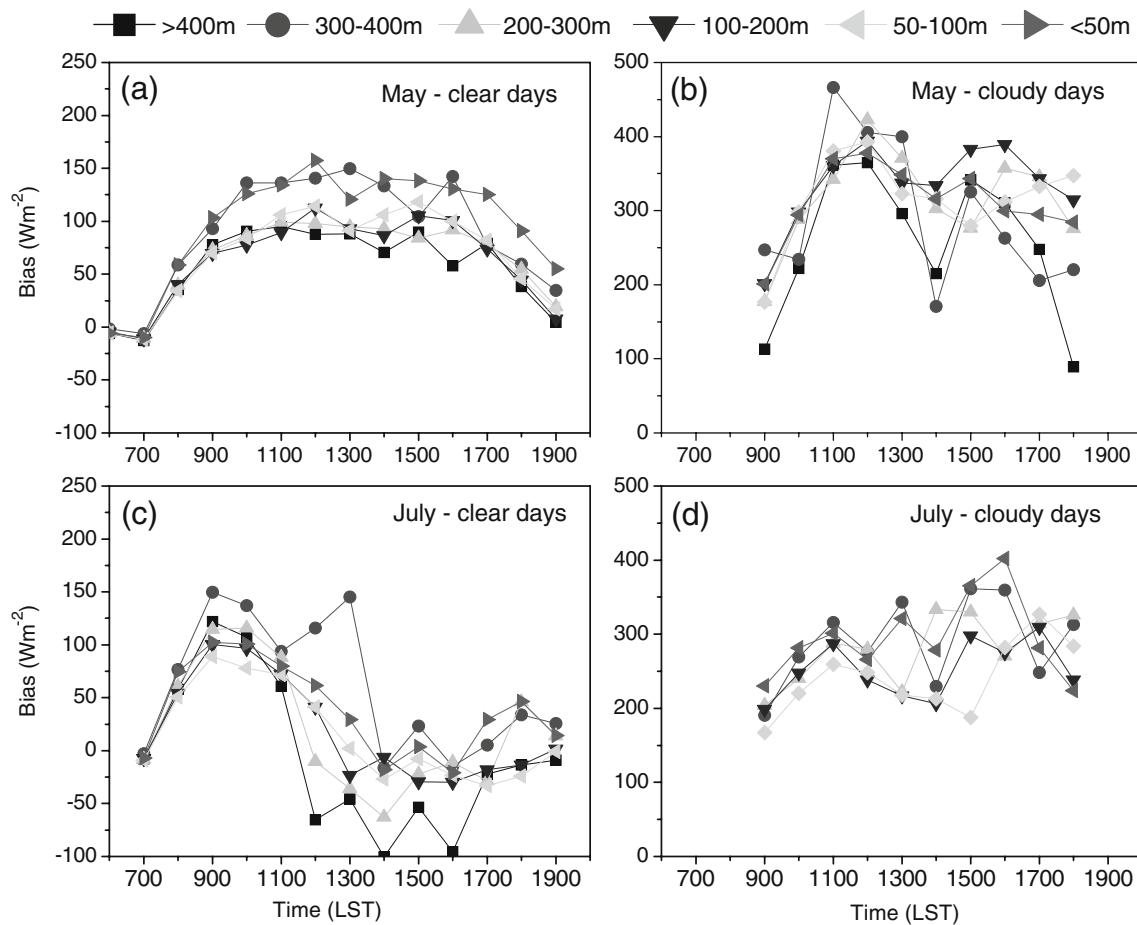


Fig. 6 Solar radiation bias during the clear days (a and c) and cloudy days (b and d) for May and July, respectively

values and observations for certain cloud-free days. This emphasized the need to look into other factors that affect the solar irradiance at the surface, such as aerosol. The aerosols are introduced in the atmosphere by both natural and anthropogenic factors, such as forest fires and urban pollution. There were several wild fires in southern Georgia and northern Florida between mid April and June which started on April 13. Daily solar irradiance at the surface bias during the fire showed (Fig. 7a) consistently a high positive bias for Nahunta (northeast of major fire), Homerville (west of the fire), and Alma (north of the fire). The daily bias in May exceeded 200 W m⁻² at Nahunta and Homerville. The month of May was characterized by less rain and low soil moisture conditions, conducive for these fire events. The AEMN observations for May showed AEMN station averaged accumulated rainfall of 15.05 mm while ARW predicted 9.5 mm of rainfall at those locations. The volumetric soil moisture decreased from 25% to 15% since the beginning of the fire until end of May, indicating a continued drying effect. The MODIS aerosol optical depth observations over the study area were available for several days in May. A few days from April and June, as indicated

in Fig. 9a (with vertical bars), were also considered for the analysis. 26 cloud-free days data were used to examine the relationship between the radiation bias, 2-m temperature bias and AOD. The bin-averaged radiation bias and temperature bias for various AOD bins (Fig. 7b) showed a systematic increase with the AODs above 0.2. While considering all AEMN data, the radiation bias and temperature bias increased from 100 to 250 W m⁻² and 2 to 4 K, respectively, for an associated increase in AODs between 0.2 and 2. The biases at elevation class 6 (coastal stations) were further enhanced. The smoke plume was also transported to other areas inland, as shown here.

The southeasterly winds during the fire carried the smoke plume towards Atlanta and the visibility was significantly reduced during the third week of May. An analysis of individual days data during this period indicated that model predicted clear sky conditions. However, AEMN observations indicated a significant hourly solar irradiance at the surface bias up to 400 W m⁻². The Moderate Resolution Imaging Spectroradiometer (MODIS) AOD increased over north Georgia as the plume got advected by the south easterly wind. The relationship between the

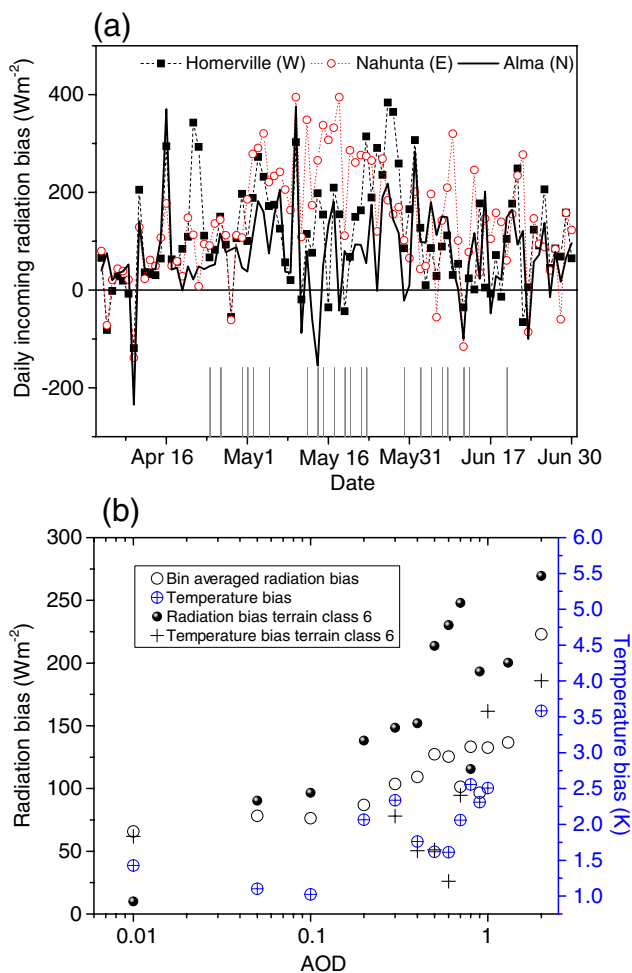


Fig. 7 Daily average radiation bias for three locations located east, west and north of Georgia forest fires in 2007 (a). Bin-averaged solar irradiance at the surface and 2-m temperature biases as a function of MODIS AOD (b) based on 26 clear days, as indicated with vertical lines in a

model radiation bias, 2-m temperature bias during the daytime hours and AODs were examined for May 20 2007 for several AEMN stations (Fig. 8). The results showed high (>0.1) AODs over regions where the smoke plume was advected; to middle Georgia on May 20 (Fig. 8c) and over to Atlanta on May 22. The anticyclonic conditions during this period were conducive for the stagnation of smoke and, thus, lead to poor visibility in the lower boundary layer. The AEMN stations that were located close to the origin of fire and in the plume path (Region A indicated in the figure) showed average radiation biases of 261 W m⁻² (at Nahunta to the east) and 149.7 W m⁻² (at Homerville to the west side), respectively. The daytime positive temperature bias showed a close relationship with AODs. ARW did not account for the additional effects of aerosol loading due to events such as the one caused by the forest fires. An inadequate representation of aerosol and ozone attenuation was related to poor solar irradiance predicted by MM5 model (Zamora et al. 2003). These

investigators also found that the introduction of the ozone attenuation into the Dudhia (1989) scheme provided more accurate results for situations with AODs near 0.1. Our results suggest similar behavior when AODs are less than 0.1, with lower biases for both solar radiation and 2-m temperature. Errors in the prediction of solar irradiance at the surface have also contributed to a positive temperature bias for locations with high AODs.

Three zones of AODs exceeding 0.1 are identified on May 20 (Fig. 8c) as Region A with the direct effect of smoke from the fire, Region B with urban effects and Region C along the coastal areas where sea sprays could be important contributing factor. The AOD for the Atlanta urban area (Region B indicated in the Fig. 8c) showed distinctly high values, for instance 0.16 at Dunwoody, compared to the suburban locations, such as 0.11 for Griffin and 0.015 for Blue Ridge. The radiation bias for Dunwoody was 96.5 W m⁻². Rural locations had a low radiation bias (such as at Griffin 64.66 W m⁻² and Blue Ridge 58.34 W m⁻²). These results showed that for an increase in AOD above 0.1 to 0.17, the solar irradiance at the surface bias increased 20%. On May 22, the radiation bias and the 2-m temperature bias increased to 100 W m⁻² over several locations close to foothills. This was in response to the movement of smoke plume over Atlanta and increase in AODs to 0.4–1.7 (Prabha and Hoogenboom 2009). On this day, several locations showed a tenfold increase in AODs compared to May 20.

Li and Trishchenko (2001) indicated that for clear sky conditions, the aerosols introduce a cooling effect at the surface, which is three to four times higher than that at the top of the atmosphere. The results from the ARW model indicate that without the aerosol effect, the model predicted an increase in the 2-m temperature of 0.5–1.5 K for clear sky conditions. These results emphasize the need to include aerosol radiative effects in the ARW. AOD measurements during the 1999 Atlanta Supersite experiment showed a value of 0.44 ± 0.22 in Atlanta, with a corresponding average direct aerosol radiative forcing at the top of the atmosphere of -11 ± 6 W m⁻² (Carrico et al. 2003). However, the clear sky surface forcing assessment may be more complicated due to the characteristics of aerosols, and could not be left out in the radiative transfer calculations.

3.4 Relationship between the solar irradiance at the surface errors and surface predictions

One important question that arises from this analysis is how such large biases in the solar irradiance at the surface affect the surface layer and boundary layer processes, including soil conditions, air temperature, water vapor content and wind predictions. The positive radiation errors caused an increase in the positive temperature biases (Fig. 9). An excess solar

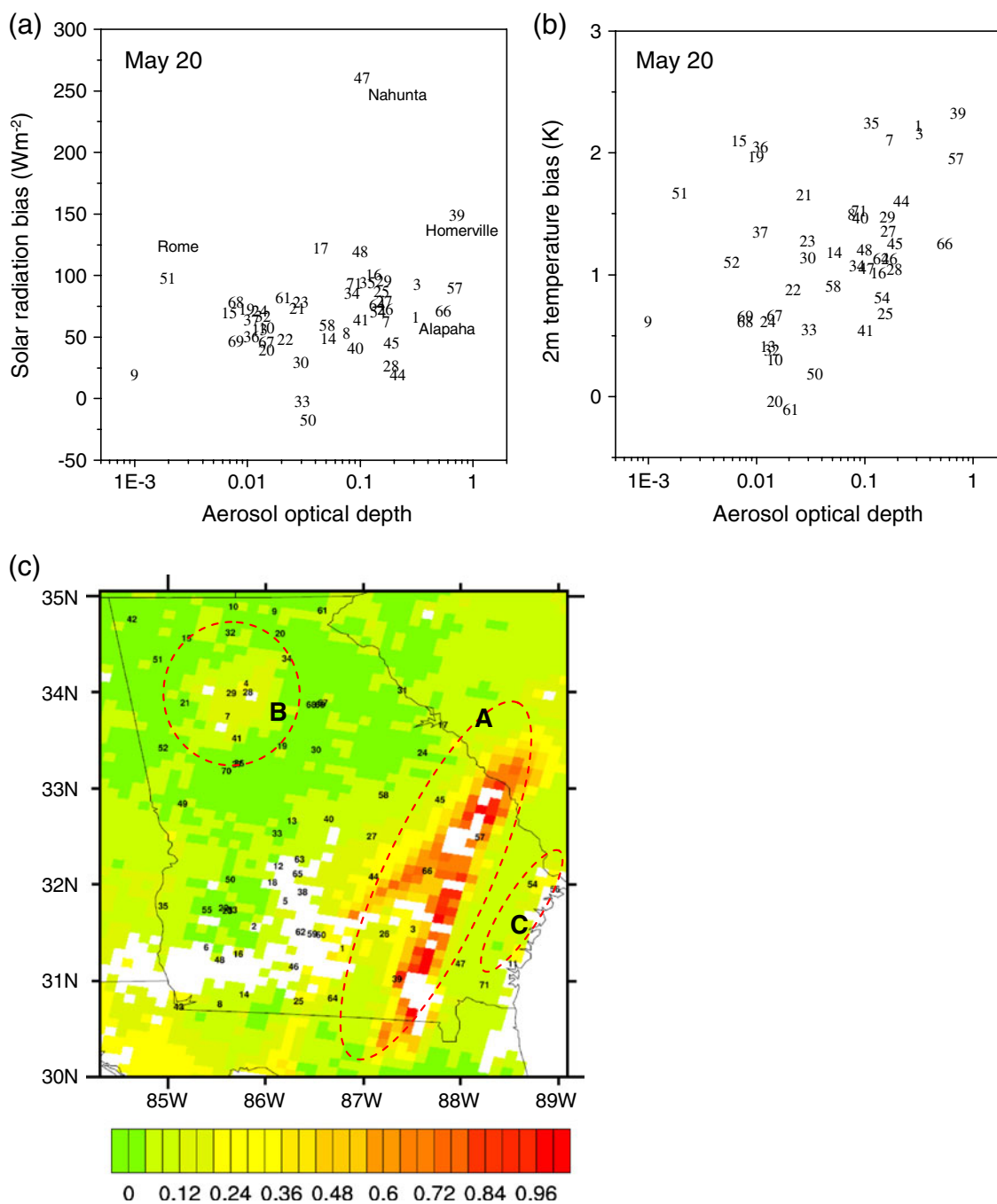


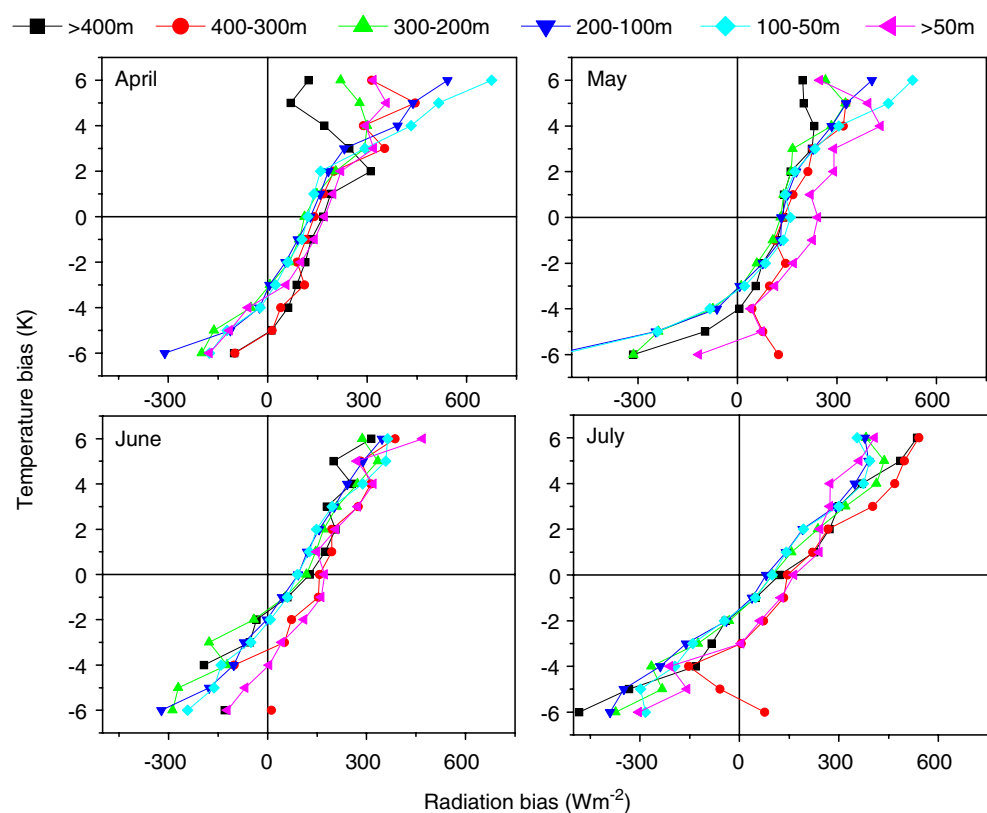
Fig. 8 Relationship between the aerosol optical depth (AOD) and solar radiation (a), 2 m temperature bias (b) on May 20. The MODIS AODs over Georgia on May 20 (c) showed spread of smoke over low-lying valleys

irradiance at the surface of 50 W m⁻² or more predicted by the ARW model corresponded to a warmer surface layer in the model when compared to the observed data. The terrain classes 300–400 m and <50 m consistently showed a positive bias that was 50–100 W m⁻² higher than other terrain classes. ARW V 2.2 did not include aerosol effects. In the present case, a direct effect was evident due to the dimming on an episodic basis (Prabha and Hoogenboom 2009). The dimming was caused by fire plume obstructing

the incoming radiation reaching the surface. The plume spread was also influenced by the large-scale weather patterns and flow stagnation in the valleys and advection effects. Since the model did not account for aerosols, this dimming was not reproduced and positive radiation bias was noted, which caused a warming at the surface, instead of a cooling in the observations.

A negative mixing ratio bias in ARW was mostly associated with the positive bias in the solar irradiance at the

Fig. 9 Relationship between hourly solar irradiance at the surface bias and 2-m temperature bias over different terrain and for April, May, June and July of 2007



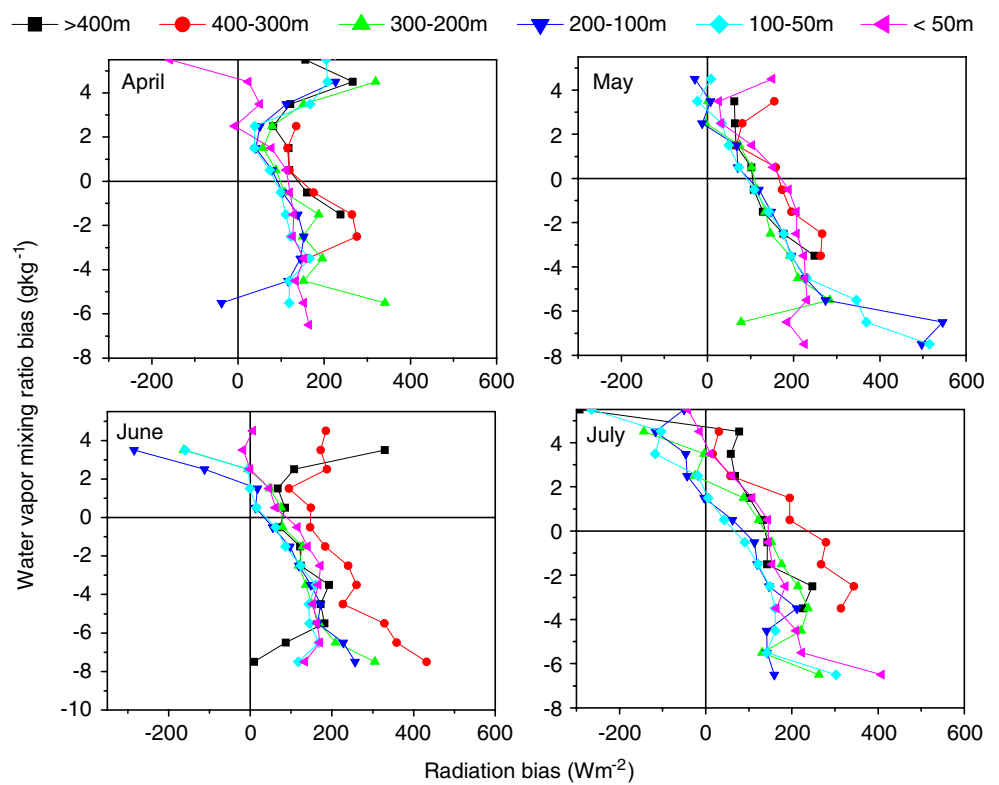
surface (Fig. 10). As more radiation reached the surface more water evaporated, however, the period of study characterized very low volumetric soil moisture content that (<15%), that less water was available and a drying effect was consistently seen, which lead to a reduction in the water vapor missing ratio. The soil moisture bias was also closely associated with radiation bias (Fig. 11), which showed a negative bias with increasing radiation bias. More solar irradiance at the surface predicted by the model resulted in a warmer (soil temperature bias is not shown) and drier soil compared to observations. Observations indicated a volumetric moisture content of 15%. It is apparent that increased irradiance in the model lead to a drier soil compared to observations. This indicates that model predicted more drought conditions than in the observations. The wind speed bias showed a positive relationship with the radiation bias (Fig. 12). The wind speed predicted by the model increased for increasing errors in the solar radiation, indicating that more radiation in the model generally contributed to more heating at the surface, resulting in strong surface layer turbulence that generated more wind. However, the wind speed and radiation error relationship is more complicated as increase in wind speed may also increase likelihood for advection of cold dry/warm wet air depending on the continental/maritime weather systems. These results demonstrated that there is a strong relationship between the surface layer temperature, mixing ratio and wind speed bias in the model and the irradiance bias. These results may have

implications for climate studies that do regional downscaling with the ARW model. A prolonged drying and warming effect artificially produced in the model which does not take into account of the fire events may eventually influence the downscaled climate.

4 Summary and conclusions

A detailed evaluation of hourly solar irradiance at the surface simulated by the Advanced Research Weather Research and Forecasting Model (WRF-ARW) was conducted for Georgia for the months of April, May, June, and July of 2007. The dependence of model bias on the amount of cloudiness, and aerosol optical depth were investigated for cloudy and cloud-free conditions respectively. It is demonstrated that observational data from in situ AEMN, and remotely sensed observations including MODIS cloud and aerosol observations could be used to investigate the failure of the model in predicting accurate solar irradiance at the surface. Results from this study suggest that there was a significant dimming effect during the month of May 2007 for all the low-lying AEMN locations in Georgia, causing a reduction in solar radiation for cloud-free days. The dimming effect contributed to a cooler, relatively wetter, and less windy surface layer compared to observations,

Fig. 10 Relationship between hourly the radiation bias and water vapor mixing ratio bias for April, May, June and July of 2007



disturbing the total energy balance at the surface. The following are the main conclusions of this study:

1. The errors of predicted solar irradiance at the surface and 2-m temperature were closely associated with the observed cloudiness as evident from the analysis with MODIS cloud optical depth and AEMN observations.
2. A systematic positive model bias of 50–100 W m⁻² during the morning hours and a negative model bias of

similar magnitude during the afternoon hours were characteristics of clear days. The radiation bias, however, increased with the amount of cloudiness in the observations.

3. Additional solar irradiance bias in the model were noticed when aerosols were present over the model domain during the clear days that characterized maximum solar radiation errors (100 W m⁻² to

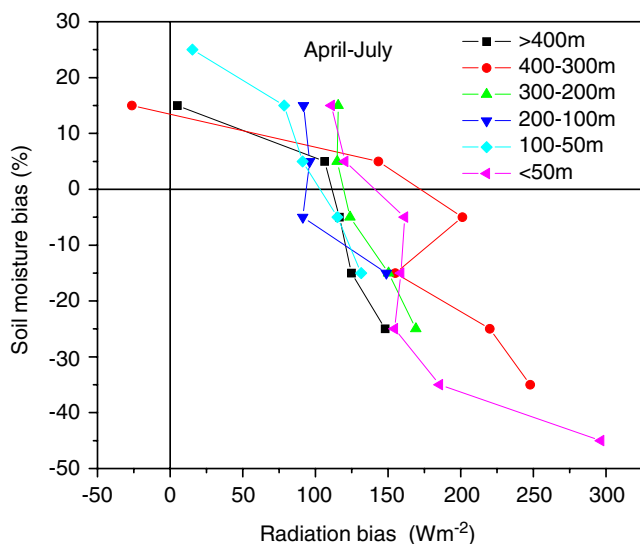


Fig. 11 Relationship between soil moisture bias and the radiation bias during 900–1700 LST over different terrain for April–July of 2007

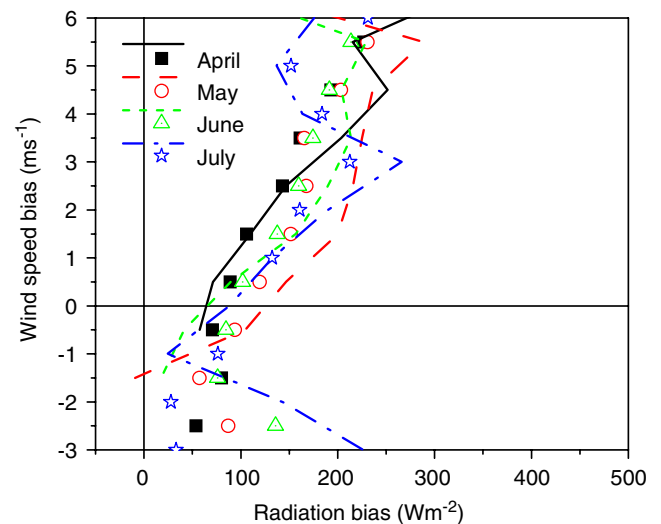


Fig. 12 Relationship between wind speed bias and the radiation bias during 900–1700 LST over AEMN stations at coastal areas (*lines*) and for all AEMN locations (*symbols*) for April, May, June, and July of 2007

250 W m⁻²). This was attributed to a fire emission induced dimming effect (from less radiation at the surface), which also leads to 2-m temperature errors (2–4 K) in the model.

4. The errors for the predictions of 2-m temperature and mixing ratio increased with the solar irradiance at the surface errors, leading to a warmer and drier model surface with higher wind speeds compared to the observations.
5. It is shown that episodic fire events during 2007 showed a significant reduction in the irradiance observed in south Georgia, which lead to a dimming effect at the surface

These results ultimately have an impact for regional scale downscaling with the ARW model, both for cloudy and clear sky situations. The inherent model bias could be corrected by conducting short-term verification studies with co-located observations. However, the inclusion of additional scattering and absorption in the model might be necessary when aerosols are present. The focus in this study was only on evaluation of the incoming shortwave radiation. Further evaluations of all components of radiation fluxes are a necessary step for future studies. Further investigations are underway focusing on different aspects of this important problem, which could have serious consequences for both weather and climate predictions.

List of symbols and descriptions

| Symbol | Parameter description |
|-----------------|----------------------------------|
| z | Height above the surface |
| μ | Cosine of the solar zenith angle |
| S_0 | Solar constant |
| dS_{cs} | Cloud scattering/reflection |
| dS_{ca} | Cloud absorption |
| dS_c | Clear air scattering |
| dS_a | Water vapor absorption |
| $R_c (\mu S_0)$ | Clear sky irradiance |
| R_o | Observed irradiance |
| F_c | Fractional cloud cover |
| R | Correlation coefficient |
| COT | Cloud optical depth |
| AOD | Aerosol optical depth |

Acknowledgments This study was funded by a partnership with the USDA Risk Management Agency and by a Seed Grant from the College of Agricultural and Environmental Sciences, the University of Georgia. Support for this project was provided by the Developmental Testbed Center (DTC). The DTC Visitor Program is funded by the National Oceanic and Atmospheric Administration, the National Center for Atmospheric Research and the National Science Foundation. Discussions with Dr. Jimmy Dudhia, National Center for Atmospheric Sciences are acknowledged. First author is also grateful to the Director, Indian Institute

of Tropical Meteorology (IITM) for providing continued support to complete this study.

References

- Beljaars ACM, Viterbo P, Miller M, Betts A (1996) The anomalous rainfall over the United States during July 1993: sensitivity to land surface parameterization and soil moisture anomalies. *Mon Wea Rev* 124:362–383
- Betts A, Chen F, Mitchell K, Janjic Z (1997) Assessment of the land surface and boundary layer models in two operational versions of the NCEP Eta Model using FIFE data. *Mon Wea Rev* 125:2896–2915
- Brutsaert WH (1982) *Evaporation into the atmosphere: theory, history and applications*. Rediel, Boston
- Carrico CM, Bergin MH, Xu J, Baumann K, Maring H (2003) Urban aerosol radiative properties: measurements during the 1999 Atlanta Supersite experiment. *J Geophys Res.* doi:10.1029/2001JD001222
- Chen F, Dudhia J (2001a) Coupling an advanced land surface-hydrology model with the Penn State-NCAR MM5 modeling system: Part I: model implementation and sensitivity. *Mon Wea Rev* 129(4):569–585
- Chen F, Dudhia J (2001b) Coupling an advanced land surface-hydrology model with the Penn State-NCAR MM5 modeling system: Part II: preliminary model validation. *Mon Wea Rev* 129(4):587–604
- Chen F, Manning KW, LeMone MA, Trier SB, Alfieri JG, Roberts R, Tewari M, Niyogi D, Horst TW, Oncley SP, Basara JB, Blanken PD (2007) Description and evaluation of the characteristics of the NCAR high-resolution land data assimilation system. *J Appl Meteor Climatol* 46:694–713
- Cheng WYY, Steenburgh WJ (2005) Evaluation of surface sensible weather forecasts by the WRF and the Eta Models over the Western United States. *Wea. and For.* 20, 812–821
- Dudhia J (1989) Numerical study of convection observed during the Winter Monsoon Experiment. *J Atmos Sci* 46:118–133
- Ek, MB, Mitchell KE, Lin Y, Rogers E, Grummann P, Koren V, Gayno G, Tarpley JD (2003) Implementation of Noah land-surface model advances in the NCEP operational mesoscale Eta model. *J. Geophys. Res.*, 108 (D22): No. 8851
- Guichard F, Parsons DB, Dudhia J, Bresch J (2003) Evaluating mesoscale model predictions of clouds and radiation with SGP ARM data over a seasonal timescale. *Mon Wea Rev* 131:926–944
- Gustafson WI, Chapman EG, Fast JD, Easter RC, and Ghan SJ (2006) Effect of cloud-aerosol-chemistry interactions on aerosol and cloud optical depths in eastern Pennsylvania during August 2004. 7th Annual WRF User's Workshop, 19-22 June 2006, Boulder, CO
- Hansen JE, Sato M, Ruedy R (1997) Radiative forcing and climate response. *J Geophys Res* 102:6831–6864
- Hoogenboom G (2005) The Georgia Automated Environmental Monitoring Network: experiences with the development of a state-wide automated weather station network. Proceedings of the 13th Symposium on Meteorological Observations and Instrumentation & 15th Conference on Applied Climatology, American Society of Meteorology, Boston, MA (Abstracts)
- Iqbal M (1983) *An introduction to solar radiation*. Academic, 390pp
- Kaufman YJ, Tanre D, Bouchier O (2002) A satellite view of aerosols in the climate system. *Nature* 419:215–223
- LeBaron J, Dirmhirn I (1983) Strengths and limitations of the Liu and Jordan model to determine diffuse radiation from global irradiance. *Solar Energy* 31:167-172.11
- Li Z, Trishchenko A (2001) Quantifying the uncertainties in determining SW cloud radiative forcing and cloud absorption due to variability in atmospheric conditions. *J Atmos Sci* 58:376–389

- Mesinger F, DiMego G, Kalnay E, Mitchell K, Shafran P, Ebisuzaki W, Jović D, Woolen J, Rogers E, Berbery EH, Ek MB, Fan Y, Grumbine R, Higgins W, Li H, Manikin G, Parish D, Shi W (2006) North American Regional Reanalysis. *Bull Am Meteorol Soc* 87(3):343–360
- Pepler RA, Bahrman CP, Barnard JC, Campbell JR, Cheng MD, Ferrare RA, Halthore RN, Heilman LA, Hlavka DL, Laulainen NS, Lin CJ, Ogren JA, Poellot MR, Remer LA, Sassen K, Spinhirne JD, Splitt ME, Turner DD (2000) ARM Southern Great Plains Site Observations of the Smoke Pall Associated with the 1998 Central American Fires, 81:2563–2591
- Prabha TV, Hoogenboom G (2009) Observed dimming effect during a forest fire in the southeastern United States and the role of aerosols. *Geophys Res Lett* 36:L11806. doi:10.1029/2009GL038435
- Raman S, Sims A, Ellis R, Boyles R (2005) Numerical simulation of mesoscale circulations in a region of contrasting soil types. *Pure Appl Geophys* 162:1689–1714
- Ramanathan V, Crutzen PJ, Kiehl JT, Rosenfeld D (2001) Aerosols, climate, and the hydrological cycle. *Science* 294:2119–2123
- Remer LA, Kaufman YJ, Tanré D, Mattoo S, Chu DA, Martins JV et al (2005) The MODIS aerosol algorithm, products and validation. *J Atmos Sci* 62:947–973
- Rosenfeld D, Lensky IM (1998) Satellite-based insights into precipitation formation processes in continental and maritime convective clouds. *Bull Amer Meteor Soc* 79:2457–2476
- Skamarock WC, Klemp JB, Dudhia J, Gill DO, Barker DM, Wang W, Powers JG (2005) A description of the Advanced Research WRF version 2. NCAR Tech. Note TN-468-STR, 88pp
- Soler A (1990) Dependence on latitude of the relation between the diffuse fraction of solar radiation and the ratio of global-to-extraterrestrial radiation for monthly average daily values. *Sol Energy* 44:297–302
- Thornton PE, Running SW (1999) An improved algorithm for estimating incident daily solar radiation from measurements of temperature, humidity, and precipitation. *Agric For Meteorol* 93:211–228
- Trishchenko A, Li Z (1998) Use of ScaRaB measurements for validating a GOES-based TOA radiation product. *J Appl Meteor* 37:591–605
- Zamora RJ, Solomon S, Dutton EG, Bao JW, Trainer M, Portmann RW, White AB, Nelson DW, McNider RT (2003) Comparing MM5 radiative fluxes with observations gathered during the 1995 and 1999 Nashville southern oxidants studies. *J Geophys Res* 108:4050. doi:10.1029/2002JD002122